# Modeling dynamics of an electro-hydraulic servo actuated manipulator: A case study of a forestry forwarder crane

Pedro Miranda La Hera
*Swedish University of Agricultural Sciences*
*Sweden, 90183*
Email: xavier.lahera@tfe.umu.se

Daniel Ortiz Morales
*Applied Physics and Electronics*
*Umeå University*
*Sweden, 90187*
Email: daniel.ortiz.morales@tfe.umu.se

***Abstract*—System modeling and parameters estimation are key elements to realize model-based control. Here, we present a discussion of modeling dynamics of a forestry forwarder crane, for which standard Euler-Lagrange formulations are used to describe its equations of motion. To calibrate this model according to experimental data, we perform parameter estimation based on the method of least squares. This procedure allows identifying various unknown parameters, which are related to the inertias, masses, location of center of masses, and friction forces coefficients. The results of simulation tests show a significant correspondence between measured and estimated variables, validating our modeling approach.**

## I. Introduction

Modern forestry operations use state-of-art systems and high-tech machinery to meet the mechanical and engineering challenges of harvesting and logging trees in a safe and environmentally responsible manner. The cranes of these machines are an especial type of mechanical manipulators, which employ hydraulic actuation to produce motions. They are engineered to be manually maneuvered by joysticks, having the human operator as the control unit. During daily work, the driver is demanded to perform various tasks simultaneously, which include visualization, recognition, selection, controlling the crane, and positioning the vehicle. This level of work demand is stressful, since the operator has to deal with an excess of information, and take various decisions at high pace.

As an attempt to support human drivers, and in view of increasing the machine productivity [1], forestry based industry and researchers have analyzed the possibility to automate the routine motions performed in these tasks [2], [3]. The forwarder family of cranes used for logging has been established as a benchmark platform to understand the fundamental challenges of designing this (semi) automatic solution. From the industrial point of view, crane manufacturers have entrepreneur the design of forwarder cranes that can support the implementation of feedback control systems [4]. Researchers, on the other hand, have provided different solutions regarding automatic control design, study of human crane operation, and trajectory planning techniques. Many of these concepts have been experimentally validated in modern laboratories dedicated to the development of future forestry technologies [5], [6], [7], [8].

Formally, forwarder cranes can be regarded as electro-hydraulically actuated mechanical systems. Theoretically, control design for such systems has proven to be challenging, due to the complex nonlinear nature of the process dynamics. In literature, we recognize the establishment of two well defined brands of development for these systems. On one hand, there exist a vast number of publications with quite mature content regarding modeling and controller design for hydraulic servo systems. Such terminology is attributed to the interconnection between valve and cylinder (or rotator), and the main objective is to control the actuator dynamics, e.g. [9], [10], [11], [12], [13], [14]. On the other hand, we have hydraulic manipulators, for which mainly model-free controllers, resembling conventional decentralized joint control, are found [15], [16], [17], [6], [8], [18], [7]. This class of controllers are usually desirable due to their simplicity of implementation. However, experimental studies reveal that their efficiency is limited to joint trajectories with slow velocity profiles [17]. As the speed of motion reaches high (human) profiles, or when the payload changes dramatically, they lack of damping capabilities and stability.

To attain improving performance, it is of interest to apply model-based motion control strategies, employing models of robot kinematics and dynamics [19]. Within this context, modeling and parameters identification are key elements to realize such a design. Therefore, the initial interest is to verify that, despite the complex mechanical structure and hydraulic hardware, standard engineering procedures for robot modeling and parameter estimation are applicable for describing and simulating dynamics of these machines. The following presentation can be regarded as a technical report of results along these lines, which presents a detailed review of our experience modeling dynamics of the mechanics of a forwarder crane and its experimental validation.

## II. Modeling

The manipulator used for our study is a downsized version of a typical forwarder crane, but similar in configuration

and dynamics (see Fig. 1). The machine is equipped with specialized equipment to realize various experimental studies, as it is fully described in [15], [5].

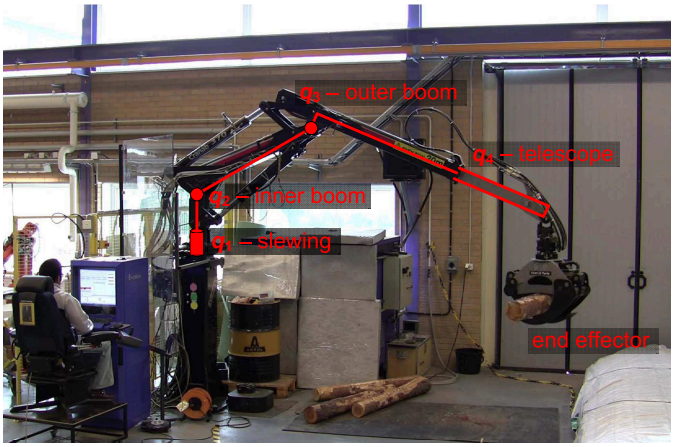


Fig. 1. Laboratory crane installed at the Department of Applied Physics and Electronics, Umeå University.

### A. Kinematic modeling

The configuration of the manipulator resembles a serial kinematic chain with a telescopic boom at the end link. The forward kinematics can be conveniently expressed using the Denavit-Hartenberg (DH) convention [19], where each link configuration is represented by the homogeneous transformation

$$A_i = \text{Rot}_{z,\theta_i}\,\text{Trans}_{z,d_i}\,\text{Trans}_{x,a_i}\,\text{Rot}_{x,\alpha_i}\,, \tag{1}$$

parameterized by joint angle $\theta_i$, link offset $d_i$, link length $a_i$, and link twist $\alpha_i$. Table I gives a summary of the geometrical parameters used to form the DH convention, when the reference frames is assigned as shown in Fig. 2[1].

TABLE I
DH PARAMETERS

| Link $i$ | $\theta_i$ [rad] | $d_i$ [m] | $a_i$ [m] | $\alpha_i$ [rad] |
|---|---|---|---|---|
| 1 | $q_1(t)$ | 2.202 | 0 | $\pi/2$ |
| 2 | $q_2(t)+\theta_{2,0}$ | 0 | 1.4 | 0 |
| 3 | $\pi/2+q_3(t)-\theta_{2,0}$ | 0 | 0.104 | $\pi/2$ |
| 4 | 0 | $d_{4,0}+q_4(t)$ | 0 | $-\pi/2$ |
| Constants: $\theta_{2,0}=0.1192\,\text{rad}$, $d_{4,0}=1.813\,\text{m}$ | | | | |

The Cartesian position of the boom tip with respect to the base frame of the robot is defined by

$$\begin{bmatrix} x \\ y \\ z \end{bmatrix} = \begin{bmatrix} I_{3\times3} & 0_{3\times1} \end{bmatrix} T_4^0 \begin{bmatrix} 0_{3\times1} \\ 1 \end{bmatrix}, \tag{2}$$

$$\text{where} \quad T_4^0 = A_1(q_1)A_2(q_2)A_3(q_3)A_4(q_4)\,.$$

[1]These parameters are taken from the CAD models provided by the manufacturer of the machine

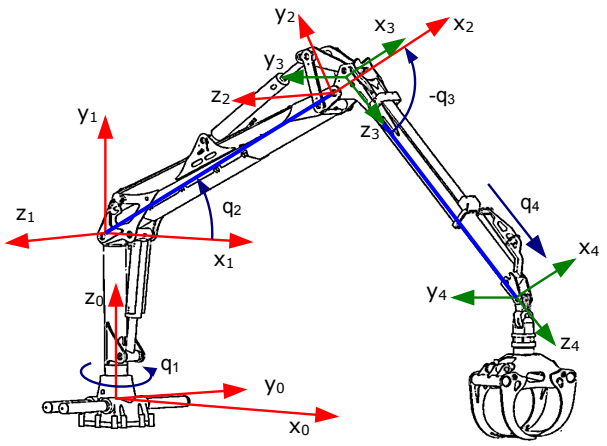


Fig. 2. Reference frames to specify the DH convention. The angular motion is measured positive when the motion is counterclockwise.

### B. Dynamics modeling

We apply the Euler-Lagrange equation as a formalism used to systematically describe the robot dynamics [19]. This procedure leads to a second order set of differential equations of the form

$$M(q)\ddot{q} + C(q,\dot{q})\dot{q} + G(q) = \tau, \tag{3}$$

where $M(q)$ denotes a symmetric and positive-definite matrix of inertias, $G(q)$ the gravity vector, $C(q,\dot{q})$ the matrix of Coriolis forces, and $\tau$ the joint torques.

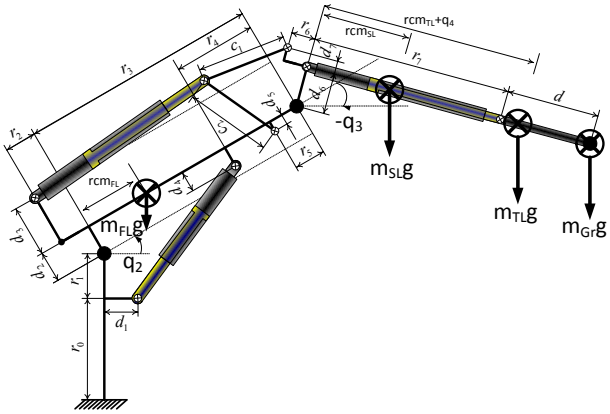


Fig. 3. Crane dimensions and masses description in the sagittal plane.

Considering motions in the plane $XZ$, as shown in the schematics of Fig. 3, the model (3) takes the form

$$M(q,\theta)\begin{bmatrix} \ddot{q}_2 \\ \ddot{q}_3 \\ \ddot{q}_4 \end{bmatrix} + C(q,\dot{q},\theta)\begin{bmatrix} \dot{q}_2 \\ \dot{q}_3 \\ \dot{q}_4 \end{bmatrix} + G(q,\theta) = \begin{bmatrix} \tau_2 \\ \tau_3 \\ F_4 \end{bmatrix}, \tag{4}$$

where $q = [q_2, q_3, q_4]^T$, i.e. the slewing angle $q_1$ is not considered, and $\theta$ represents the crane inertial parameters. In

addition, and assuming no frictional forces, the set of equations in (4) can be transformed and represented linearly in the elements of the base parameters $\theta$, i.e.

$$\varphi(q(t), \dot{q}(t), \ddot{q}(t)) \cdot \theta = \tau, \tag{5}$$

where $\varphi(\cdot)$ denotes the regressor written in terms of the measurable variables $[q, \dot{q}, \ddot{q}]$, $\theta = [\theta_1, ..., \theta_7]^T$ the minimum set of inertial parameters, and $\tau$ the vector of generalized input torques and forces, which is equal to the right hand side of (4).

### C. Modeling friction forces

To model friction forces we consider the static Coulomb - viscous friction formulated as

$$\tau_i^F = f_{c,i} \cdot \mathrm{sgn}(\dot{q}_i) + f_{v,i} \cdot \dot{q}_i, \tag{6}$$

where $i = \{2, 3, 4\}$, and corresponds to the $i$th link of the robot, $f_v$ and $f_c$ denote the viscous and Coulomb friction coefficient respectively [20]. Hydraulic systems exhibit appreciable asymmetric friction forces, i.e. the constant parameters used to represent friction change according to the direction of motion, i.e.

$$f_v = \bar{f}_v + \Delta f_v \cdot \mathrm{sgn}(\dot{q}), \tag{7}$$
$$f_c = \bar{f}_c + \Delta f_c \cdot \mathrm{sgn}(\dot{q}), \tag{8}$$

where the terms with a $\bar{bar}$ denote the mean values, and their variational values $\Delta$ depend on the direction of motion given by the $\mathrm{sgn}(\dot{q})$. Introducing the above equations into the general form (6) yields a more complete model for friction forces:

$$\tau_i^F = \bar{f}_{c,i} \cdot \mathrm{sgn}(\dot{q}_i) + \Delta f_{c,i} + \bar{f}_{v,i} \cdot \dot{q}_i + \Delta f_{v,i} \cdot |\dot{q}_i|, \tag{9}$$

which is able to capture the most relevant effects of the nonlinear friction phenomena.

### D. Including friction forces into the model (5)

Due to the linearity of the friction parameters in (9), i.e.

$$\tau_i^F = \underbrace{[\mathrm{sgn}(\dot{q}_i) \;\; 1 \;\; \dot{q}_i \;\; |\dot{q}_i|]}_{\varphi_i^f} \cdot \underbrace{\begin{bmatrix} \bar{f}_{c,i} \\ \Delta f_{c,i} \\ \bar{f}_{v,i} \\ \Delta f_{v,i} \end{bmatrix}}_{\theta_i^f}, \tag{10}$$

the introduction of friction forces into the linear model (5) is straightforward. To show this, we form a complete set of friction forces for the three links considered, i.e. $q = [q_2, q_3, q_4]^T$, as follows

$$\tau^F = \underbrace{\begin{bmatrix} \varphi_2^f & 0 & 0 \\ 0 & \varphi_3^f & 0 \\ 0 & 0 & \varphi_4^f \end{bmatrix}}_{\varphi^f} \cdot \underbrace{\begin{bmatrix} \theta_2^f \\ \theta_3^f \\ \theta_4^f \end{bmatrix}}_{\theta_f}, \tag{11}$$

where the zero vectors have dimension 1-by-4. Considering that frictions forces act opposed to the torques in the right hand side of (5), a more complete linear model to be used for parameter estimation is given by

$$[\varphi(q(t), \dot{q}(t), \ddot{q}(t)) \quad \varphi_f(\dot{q}(t))] \cdot \begin{bmatrix} \theta \\ \theta_f \end{bmatrix} = \tau, \tag{12}$$

which results by the combination of (5)-(11), and is linear in its unknown parameters.

### E. Mapping cylinder forces to joint torques

Using the geometry of the machine, the mapping between the linear cylinder's pistons displacements and joint angles can be found. This mapping $x_i = f(q_i)$, can be used for $a)$ deriving the joint torques, and $b)$ computing the velocity of the cylinder's piston given angular velocity. To this end, we begin by considering the virtual work principle [19], to define that

$$\tau_i \cdot dq_i = F_i \cdot dx_i, \tag{13}$$

which yields an equality for the joint torque as

$$\tau_i = F_i \cdot \frac{dx_i}{dq_i}, \tag{14}$$

for the links $i = [2, 3]$, as required in (4)[2].

The actuators forces (see Fig. 4) can be calculated as [13]

$$F_i = A_{A,i} p_{A,i} - A_{B,i} p_{B,i}, \quad i = \{2, 3, 4\}, \tag{15}$$

where $A_{A,i}$, $A_{B,i}$ denote the areas of chambers $A$, $B$ respectively, and $p_{(\cdot)}$ the measurements of their corresponding pressures, which in the machine are available through pressure transducers.

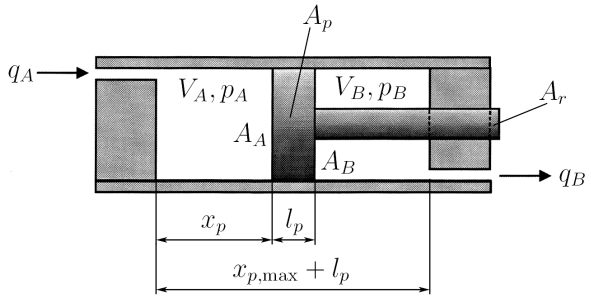


Fig. 4. Hydraulic single-rod cylinder [13].

*1) Finding the relation $x_2(q_2)$:* In order to calculate the change of linear piston displacement $x_2$ as a function of the measured joint angle $q_2$, we apply the following relation

$$x_2(q_2) = \sqrt{j_1^2 + j_2^2 - 2 j_1 j_2 \cos\left(\frac{\pi}{2} - \varphi_4 + \varphi_3 + q_2\right)}, \tag{16}$$

which is derived by the geometry drawn in Fig. 5.

[2]Recall that the telescopic displacement $q_4$ is linear, and therefore only its cylinder force $F_4$ is needed in the dynamics (4)

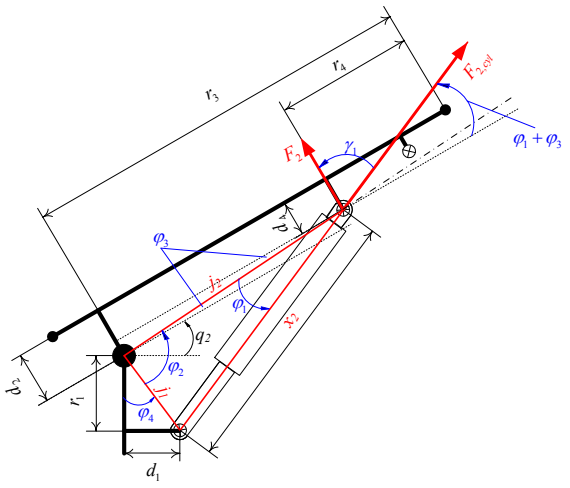


Fig. 5. Geometry of the first link as function of the cylinder opening $x_2$. The schematics show the portion related to the motion of $q_2$ from Fig. 3

*2) Finding the relation $x_3(q_3)$:* The schematics presented in Fig. 6 allow to define the geometric relations, i.e.

$$\gamma_{21}(q_3) = \frac{\pi}{2} - \beta_1 - q_3 + \gamma_{25}, \quad (17)$$

$$s_{24}(q_3) = \sqrt{s_{22}^2 + s_{23}^2 - 2 s_{22} s_{23} \cos\left(\gamma_{21}(q_3)\right)}, \quad (18)$$

$$\gamma_{24}(q_3) = \arccos\left(\frac{c_1^2 + c_2^2 - s_{24}(q_3)^2}{2 c_1 c_2}\right), \quad (19)$$

which represent the relation of the measured angular motion $q_3$ with the mechanics driven by the second cylinder. It follows

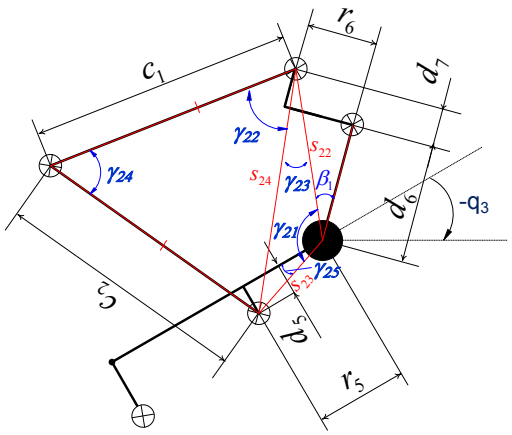


Fig. 6. Geometry of the measured angle $q_3$, with the essential mechanical components that produce its motion. The schematics show the portion related to the motion of $q_3$ from Fig. 3.

from the schematics in Fig. 7 that the linear displacement of the second cylinder can be calculated as

$$x_3(q_3) = \sqrt{s_{33}^2 + s_{31}^2 - 2 s_{31} s_{33} \cos(\gamma_{31})}, \quad (20)$$

where the coefficients $s_{33}$ and $\gamma_{31}$ are functions of $q_3$. These functions can be computed by the geometrical relations seen from both schematics in Fig. 6-7, and given by

$$\gamma_{31} = \gamma_{21} - \gamma_{32} - \arccos\left(\frac{s_{33}^2 + s_{22}^2 - c_1^2}{2 s_{33} s_{22}}\right), \quad (21)$$

$$\gamma_{32} = \arccos\left(\frac{s_{31}^2 + s_{32}^2 - s_{23}^2}{2 s_{31} s_{23}}\right). \quad (22)$$

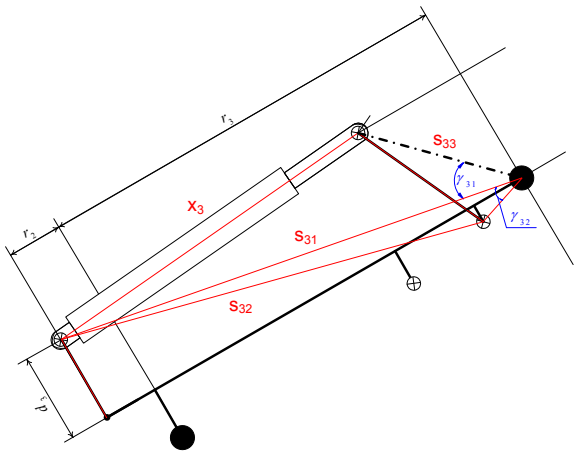


Fig. 7. Geometry of the second link cylinder. The schematics show the portion related to the motion of $q_3$ from Fig. 3.

Finally, the vector of generalized forces, in the right hand side of (12), can be computed from (14), (16), (20), as

$$\tau = \begin{bmatrix} \frac{\partial x_2}{\partial q_2} F_2 \\ \frac{\partial x_3}{\partial q_3} F_3 \\ F_4 \end{bmatrix}. \quad (23)$$

## III. Estimation of Model Parameters

Recalling that dynamics of the robot can be linearly written from (12) in the form $\Phi \cdot \Theta = \tau$, and that measurements of joint positions and input forces are recorded at each $t_i$, with $i = \{1, ..., T\}$, an overdetermined matrix of the form

$$\begin{bmatrix} \Phi(t_1) \\ \Phi(t_2) \\ \vdots \\ \Phi(T) \end{bmatrix} \cdot \Theta = \begin{bmatrix} \tau(t_1) \\ \tau(t_2) \\ \vdots \\ \tau(T) \end{bmatrix}, \quad (24)$$

can be formed for finding an estimate $\hat{\Theta}$ of $\Theta$ that fits the model (24). There are various mathematical forms to define this concept, such as the least-square estimate, which is conceptually the value of $\Theta$ that minimizes the residual of the vector $|\tau - \Phi\Theta|$, and in its most conventional form has the solution

$$\hat{\Theta} = \left(\Phi^T \Phi\right)^{-1} \Phi^T \tau = \Phi^{\dagger} \tau, \quad (25)$$

where $\Phi^{\dagger}$ denotes the pseudo-inverse of $\Phi$.

### A. Design of optimal exciting trajectories

The condition number[3] of the matrix $\Phi$ can be used as a measure for the sensitivity of the least square solution $\hat{\Theta}$, to perturbations on its elements and $\tau$. Since the elements of $\Phi(q, \dot{q}, \ddot{q})$ are somewhat trajectory dependent, it is possible to classify optimal exciting reference trajectories.

The generation of optimal (or persistently exciting) trajectories can be done by the use of finite Fourier series, yielding a periodic response, i.e. all measured signals are periodic after a transient response. The excitation trajectory for each joint is written as a finite sum of harmonic sine and cosine functions, i.e.

$$q_i(t) = q_{i,0} + \sum_{k=1}^{N} \left[ a_{i,k} \sin(k\omega_f t) - b_{i,k} \cos(k\omega_f t) \right], \quad (26)$$

with $\omega_f$ being the fundamental frequency of the Fourier series, for which the period $T_f = 2\pi/\omega_f$. Each Fourier series contains $2N_i + 1$ parameters, which can found by constrained optimization techniques. The performance criteria consists on the condition number of $\Phi$, which value is used to determine the efficiency of the matrix inversion in (25)[4]. The constraints are defined by the links limitations and saturation in velocities, as shown in table II. Examples of results of this optimization routine can be seen in Fig. 8 - 9.

TABLE II
POSITION AND VELOCITY CONSTRAINTS

| Link $i$ | $q_{i,\min}$ | $q_{i,\max}$ | $\dot{q}_{i,\min}$ | $\dot{q}_{i,\max}$ |
|---|---|---|---|---|
| 2 | $-0.45$ | 1.37 | $-0.16$ | 0.21 |
| 3 | $-2.7$ | $-0.1$ | $-0.43$ | 0.39 |
| 4 | 0 | 1.55 | $-0.67$ | 0.5 |

### B. Recording data and averaging

In the machine, the exciting trajectories are realized by decentralized PD feedback gains [15], i.e.

$$u_i = -K_p(q_i - q_i^{ref}) - K_d(\dot{q}_i - \dot{q}_i^{ref}) + F_f(\dot{q}_i), \quad (27)$$

where $K_p$ denotes the values of proportional gains, $K_d$ the values of derivative gains, and $F_f$ is a feedforward term used for avoiding the dead-zones of the control valves. The control signal $u_i$ is the electrical input level to the electro-hydraulic valve [17], and the estimation of velocities and accelerations is done by the use of Kalman filtering, as suggested in [21].

The data is recorded for various periods, and it is finally averaged to improve the signal-to-noise ratio of the measured signals.

[3]The ratio between the maximal and minimal singular values of a matrix. Large condition numbers indicate a nearly singular matrix

[4]Notice that during the optimization routine the ideal derivatives of (26) are used for the computation of the regressor $\Phi(q, \dot{q}, \ddot{q})$, and its condition number

### C. Estimation and validation of parameters $\hat{\Theta}$

Various trajectories where recorded to evaluate different ranges of motion. Considering a recursive algorithm of the least-square estimation, a set of parameters $\hat{\Theta}$ was found. Additional data sets were recorded for validation tests, two of which are presented in Fig. 8 - 9. The validation results in Fig. 10 - 11 show a comparison of the averaged measured torque $\bar{\tau}_m$, versus the torque computed by the model (12), once the values of the parameters $\hat{\Theta}$ have been estimated. We can see that major dynamics are successfully covered by the model, with minor uncertainty not captured due to unmodeled dynamics.

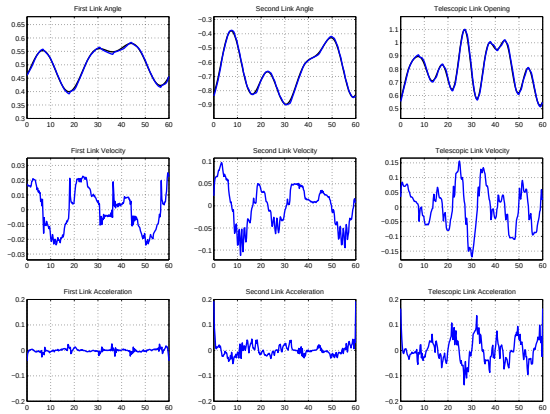


Fig. 8. First example of data used for validation. First row: Averaged trajectories in [rad]. Second row: Averaged velocity in [rad/sec]. Third row: Estimated acceleration in [rad/sec^2]. The x-axis is time in seconds.

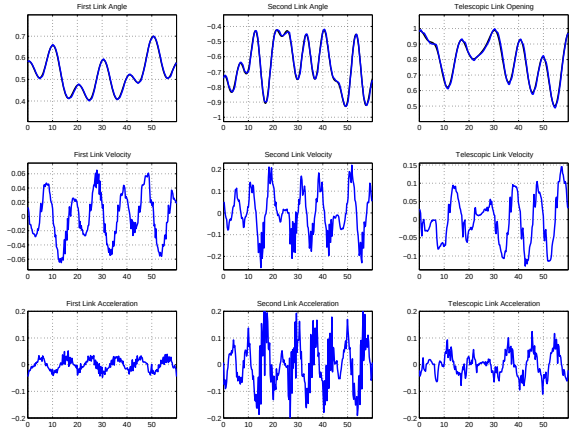


Fig. 9. Second example of data used for validation. First row: Averaged trajectories in [rad]. Second row: Averaged velocity in [rad/sec]. Third row: Estimated acceleration in [rad/sec^2]. The x-axis is time in seconds.

## IV. CONCLUSIONS

We have presented results of robot modeling and inertial parameters estimation, which were successfully carried on

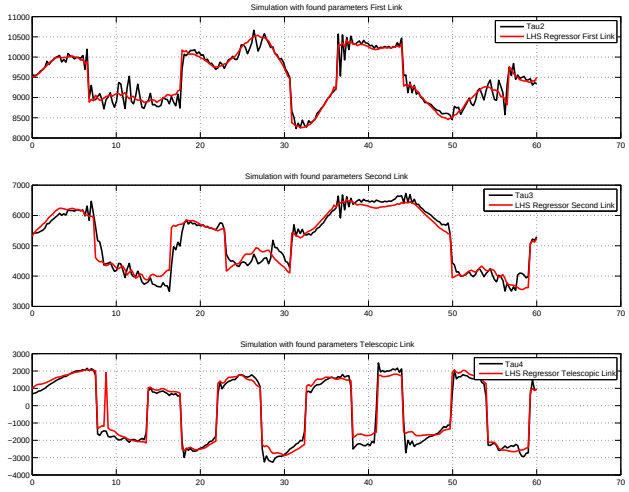


Fig. 10. Validation with the first data set from Fig. 8. The plot shows the measured averaged torque (black line) vs. estimated torque (red line), where the two graphs on top are in [Nm], and the bottom graph is in [N]. The x-axis is time in seconds.

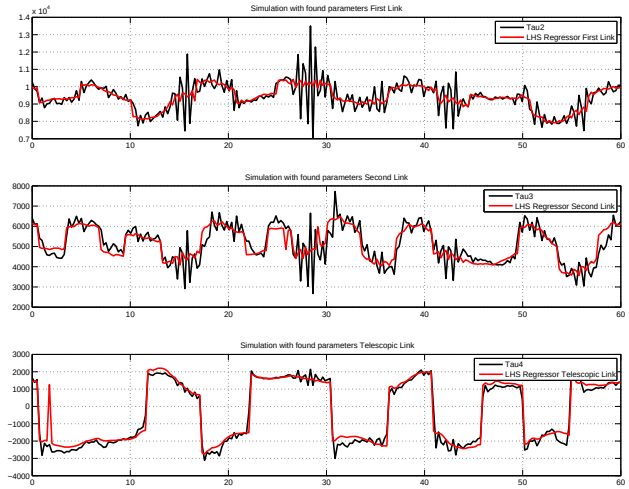


Fig. 11. Validation with the second data set from Fig. 9. The plot shows the measured averaged torque (black line) vs. estimated torque (red line), where the two graphs on top are in [Nm], and the bottom graph is in [N]. The x-axis is time in seconds.

a manipulator used in forestry machines. It is shown that despite the complex interaction between the hydraulic and mechanical processes of the robot, the system's dynamical response can be reasonably described by first principle laws. Coulomb and viscous friction forces are considered for their relevance to describe nonlinear dynamics near zero velocities. The computation of joint torques, from cylinder forces, is done by explicit calculation based on the geometry of the machine. This allows a direct calculation of the joint torques given measured hydraulic pressures.

To calibrate the model we apply an estimation method based on least squares. To produce reliable estimates, we design a set of optimal trajectories, where the optimality is referred to the inversion of the systems regressor for the least-square calculation, and measured by its condition number.

The results allow to assess the correctness of the estimated parameters, and let us conclude that despite minor differences, the model found is able to capture the most relevant dynamics involved in a motion.

## REFERENCES


[1] B. Löfgren, "Automation of forestry machines - an important piece in precision forestry," in *Proceedings of the International Precision Forestry Symposium*, Stellenbosch University, South Africa, 2006.

[2] U. Hallonborg, "Förarlösa skogsmaskiner kan bli lönsamma (unmanned forestry machines can be competitive)," Skogforsk Results, No 9, 2003.

[3] M. Brander, D. Eriksson, and B. Löfgren, "Automation of knuckleboom work can increase productivity," Skogforsk Results, No 4, 2004.

[4] (2011, June) Cranab presents an entirely new generation of cranes. [Online]. Available: http://www.cranab.se/static/en/206/

[5] A. Shiriaev, L. Freidovich, I. Manchester, U. Mettin, P. L. Hera, and S. Westerbeg, "Status of Smart Crane Lab project: modeling and control for a forwarder crane," Technical report, Department of Applied Physics and Electronics, Umeå University, 2008.

[6] M. Münzer, "Resolved motion control of mobile hydraulic cranes," Ph.D. dissertation, Aalborg University, 2002.

[7] N. P. Parchuru and J. Thati, "DSP implementation of a control algorithm for a forwarder crane," Master's thesis, Blekinge Institute of Technology, 2010.

[8] M. Linjama, "The modelling and actuator space control of flexibile hydraulic cranes," Ph.D. dissertation, Tampere University of Technology, 1998.

[9] S. Rodermond, "Modeling, identification and control of a multivariable hydraulic servo system," Master Thesis, 2006.

[10] R. V. M. Donath, "Dynamic feedback linearization for electrohydraulically actuated servosystem," in *Proceedings of the 1992 Japan/USA Symposium on Flexible Automation*, San Francisco, USA, July 1992, pp. 595–606.

[11] B. F. and B. Yao, "Adaptive robust precision motion control of single-rod hydraulic actuators with time varying unknown inertia: a case study," in *ASME International Mechanical Engineering Congress and Exposition*, Nashville, Tennessee, November 15 - 16 1999, pp. 131–138.

[12] P. L. Hera, U. Mettin, S. Westerberg, and A. Shiriaev, "Modeling and control of hydraulic rotary actuators used in forestry cranes," in *Proceedings of the 2009 IEEE International Conference on Robotics and Automation*, Kobe, Japan, May 12-17 2009, pp. 1315–1320.

[13] N. D. Manring, *Hydraulic Control Systems*, 1st ed. New York, USA: John Wiley & Sons, 2005.

[14] M. Jelali and A. Kroll, *Hydraulic Servo-Systems: Modeling, Identification and Control*, 2nd ed. Great Britain: Springer, 2004.

[15] U. Mettin and P. L. Hera, "Modeling and control design for a hydraulic forestry crane," Research Results, Department of Applied Physics and Electronics, Umeå University, 2005.

[16] P. Lawrence, F. Sassani, B. Sauder, N. Sepehri, U. Wallersteiner, and J. Wilson, "Computer-assisted control of excavator-based machines," in *International Off-Highway and Powerplant Congress and Exposition*, Milwaukee, Wisconsin, USA, September 1993, p. Document number 932486.

[17] P. La Hera, U. Mettin, I. Manchester, and A. Shiriaev, "Identification and control of a hydraulic forestry crane," in *Proceedings of the 17th IFAC World Congress*, Seoul, Korea, July 6-11 2008, pp. 2306–2311.

[18] J. Mattila and T. Virvalo, "Computed force control of hydraulic manipulators," in *5th Scandinavian Inter. Conf. On Fluid Power*, Sweden, July 6-11 1997, p. 139154.

[19] M. Spong, S. Hutchinson, and M. Vidyasagar, *Robot Modeling and Control*. New Jersey: John Wiley and Sons, 2006.

[20] H. Olsson, K. Åström, C. Canudas de Wit, M. Gäfvert, and P. Lischinsky, "Friction models and friction compensation," *European Journal of Control*, vol. 9, no. 4, pp. 176–195, 1998.

[21] P. Belanger, P. Dobrovolny, A. Helmy, and X. Zhang, "Estimation of angular velocity and acceleration from shaft-encoder measurements," *The International Journal of Robotics Research*, vol. 17, no. 11, pp. 1225–1233, 1998.